NOAA Technical Memorandum ERL ESG-22

CALIBRATION AND ACCURACY OF THE NOAA/ERL GUST PROBE SYSTEM AND INTERCOMPARISON WITH OTHER SYSTEMS

Gary G. Greenhut
Richard O. Gilmer

Environmental Sciences Group
Boulder, Colorado
October 1985

noaa NATIONAL OCEANIC AND ATMOSPHERIC ADMINISTRATION / Environmental Research Laboratories

NOAA Technical Memorandum ERL ESG-22

CALIBRATION AND ACCURACY OF THE NOAA/ERL GUST PROBE SYSTEM AND INTERCOMPARISON WITH OTHER SYSTEMS

Gary G. Greenhut
Richard O. Gilmer

Environmental Sciences Group
Boulder, Colorado
October 1985

UNITED STATES
DEPARTMENT OF COMMERCE

Malcolm Baldrige,
Secretary

NATIONAL OCEANIC AND
ATMOSPHERIC ADMINISTRATION

Anthony J. Calio,
Administrator

Environmental Research
Laboratories

Vernon E. Derr,
Director

NOTICE

Mention of a commercial company or product does not constitute an endorsement by NOAA/ERL. Use of information from this publication concerning proprietary products or the tests of such products for publicity or advertising purposes is not authorized.

CONTENTS

CALIBRATION AND ACCURACY OF THE NOAA/ERL GUST PROBE SYSTEM AND INTERCOMPARISON WITH OTHER SYSTEMS

ABSTRACT

The calibration techniques for the National Oceanic and Atmospheric Administration/Environmental Research Laboratories (NOAA/ERL) gust probe system are reviewed and the instrumental errors associated with the measurement of the fluxes of latent and sensible heat and momentum are calculated. Power spectra and cospectra of the fluctuating meteorological variables are displayed and comparisons of the eddy fluxes from the gust probe system with bulk aerodynamic calculations are reviewed. Also reviewed are comparisons of spectra and eddy fluxes from the NOAA/ERL gust probe system with those of the National Center for Atmospheric Research and the United Kingdom. Results of this report indicate that the NOAA/ERL airborne gust probe system is reliable for measuring turbulence parameters and that data obtained from the system can be used with confidence.

1. INTRODUCTION

The National Oceanic and Atmospheric Administration/Environmental Research Laboratories (NOAA/ERL) gust probe system has been used over the last decade and a half in a variety of experiments over land and over the oceans. It has proved to be a reliable method for measuring the boundary layer turbulent fluxes of temperature, moisture, and momentum and has contributed data to specialized studies of the structure of boundary layer updrafts and downdrafts (Greenhut and Khalsa, 1982; Khalsa and Greenhut, 1985). When used along with fast-response instruments that measure ozone (Pearson and Stedman, 1980) and CO_2 (Bingham and Shinn, 1983), the gust probe system has provided information on the turbulent transport of these trace species in the boundary layer (Greenhut et al., 1984; Greenhut, 1983, 1984, 1985).

The calibration and instrumental resolution of the gust probe system have been discussed in a number of reports in the past. We summarize those reports and perform a new calculation of the instrumental errors, the latter made necessary by changes in some of the electronic and mechanical components of the gust probe system since the last complete calculation over a decade ago (Grossman and Bean, 1973). In addition, we review the spectral characteristics of the gust probe system and comparisons of the eddy flux measurements with fluxes obtained using the bulk aerodynamic method. Reports

describing intercomparisons between the NOAA/ERL gust probe system and other fast-response instruments are summarized.

2. OPERATION AND CALIBRATION OF THE NOAA/ERL GUST PROBE SYSTEM

Operation of the NOAA/ERL gust probe system has been discussed by a number of authors. Bean et al. (1976), Bean and Reinking (1978), and Bean and Emmanuel (1980) describe the configuration and operation aboard large aircraft such as a DC-6 or WP-3D. Operation aboard smaller aircraft such as a Duke or Aerocommander is discussed by Gilmer and McGavin (1977) and Gilmer et al. (1978). The reader is referred to these reports for details not given here.

An updated schematic of the system when in operation aboard a NOAA WP-3D is shown in Fig. 1. The turbulence sensors are normally mounted on a boom 2.4 m in front of the nose of the aircraft. The length of the boom was chosen

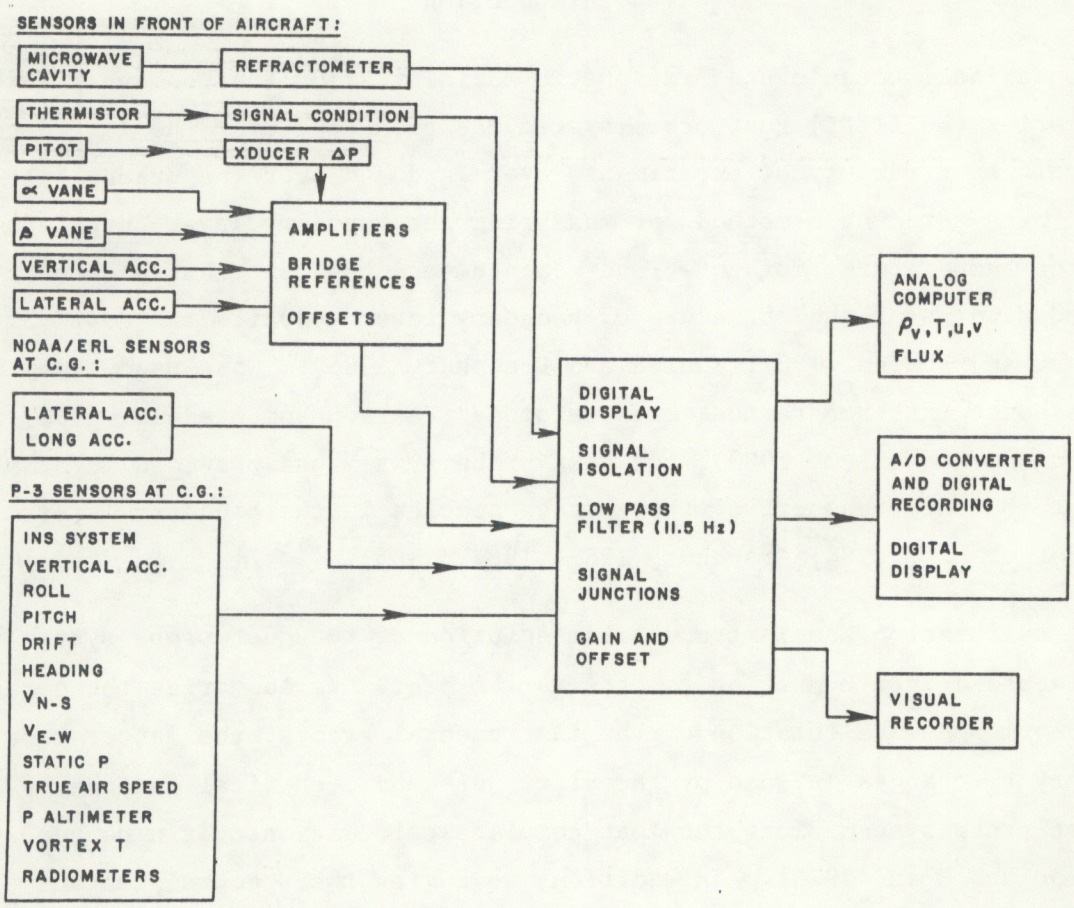

Figure 1.--Schematic of the turbulence measuring system when in use aboard a NOAA WP-3D aircraft.

to give a natural frequency of about 14 Hz when the gust probe system is mounted on it. Because the boom is mounted off-center on the P-3, extreme care is taken to control aircraft pitch, roll and yaw while the gust probe system is in operation. To avoid aliasing of the high-frequency vibrations of the probe mounts and the natural resonances of the individual sensors, a four-pole Butterworth filter is applied to all signals. The filter has a cutoff frequency of 11.5 Hz which is well below the resonant frequency of the boom. All signals must be filtered identically to avoid introducing phase lags. A sampling rate of 80 samples s^{-1} is used which is much higher than the desired upper frequency limit of 10 Hz. Additional filtering is often done during data processing, normally with a two-stage running mean filter.

The turbulence sensor package includes a small-bead thermistor for temperature measurements, a microwave refractometer cavity to detect water vapor fluctuations, and a gust probe for air velocity measurements. The operation and calibration of these instruments are discussed by Bean et al. (1976), Gilmer and McGavin (1977), Gilmer et al. (1978), and Bean and Emmanuel (1980), and are summarized and updated here.

The small-bead thermistors used on the P-3 have a high frequency cut-off of 8-10 Hz. Larger thermistors have been used in the past, e.g., on the Aerocommander, with frequency responses of up to about 3 Hz. The thermistors are directly exposed to the free air stream and are mounted so that the temperature variations of the housing do not affect the measurement of the atmospheric fluctuations. The thermistors are calibrated in a wind tunnel to correct for dynamic heating. The expression relating the ambient temperature, T_a, to the indicated temperature, T_i, is

$$T_a = T_i \, (1 - 0.20 \, K \, M^2) \qquad (°C)$$

where M is the Mach number and K is a form factor that varies from about 0.5 to 1. The dynamic heating correction is on the order of 4°C at an air speed of 100 m s^{-1} (M = 0.29). The thermistors have excellent stability; low noise and uniform characteristics allow them to be interchanged. They are constrained to operate over a 10°C range to avoid non-linearities.

The microwave refractometer measures fluctuations in the radio refractive index, n, up to frequencies on the order of 100 Hz. By combining this measurement with simultaneous measurements of temperature, T, and pitot tube static pressure, P, the fluctuations in water vapor density, ρ_v, are obtained up to at least 10 Hz using

$$\rho_v = C_1 NT - C_2 P \qquad (g\ m^{-3}) \qquad (1)$$

where

$$N = (n-1) \times 10^6 \ , \qquad (2)$$

$$C_1 = 5.81 \times 10^{-4} \quad \text{and} \quad C_2 = 4.51 \times 10^{-2}$$

(McGavin and Vetter, 1965; Bean and Dutton, 1966). The upper limit to the frequency response for ρ_v' is determined by the frequency response of measurements of the fluctuations of T and P. (Primed quantities denote the variable in a time series after the mean and linear trend have been removed.) Water flume tests of the microwave refractometer cavity indicate that it recognizes two events as independent if they are separated by 1 m. This corresponds to a frequency response of 100 Hz at an aircraft speed of 100 m s^{-1}. The cavity is made out of Invar with an effective temperature coefficient of 0.03 N $(°C)^{-1}$. The microwave refractometer is usually constrained to operate over a range of 40N to ensure adequate resolution. In the field, the cavity sensor is periodically checked for plate erosion due to salt spray and the impact of ice, and is rinsed with distilled water before and after each flight. Both temperature measurements and, to a lesser extent, microwave refractivity measurements are affected by moderate to heavy rain. Under these conditions, the time series of T' and ρ_v' should be examined carefully for spikes and other inhomogeneities before being used.

The gust probe consists of two vanes, one vertical that measures the horizontal wind perpendicular to the aircraft axis, the other horizontal that measures the vertical wind, and a centrally located pitot tube that measures the wind along the axis of the aircraft. Aircraft motion, primarily pitch, roll and yaw, and the motion of the boom are corrected for using the output of

the INS (Inertial Navigation System) and accelerometers at the aircraft center of gravity and at the gust probe. The appropriate equations are given in Sec. 3. The vanes are calibrated by hanging weights from them varying from 1 to 500 g (the gust probe is rotated by 90 deg in order to calibrate the vertical vane). The vane constant, which relates the angle of attack to the normal force on the vane, is obtained during a wind tunnel calibration. Pitch and sideslip maneuvers have been performed while the gust probe was mounted on the P-3 in order to determine the effects of flow distortion by the fuselage.

The raw parameters needed to obtain data from the gust probe system are given in Table 1. The parameters $\Delta\theta$, $\Delta\phi$, $\Delta\psi$ and Δa_z are read directly from the Inertial Navigation System aboard the aircraft. On the P-3, the static pressure, P, is obtained from the aircraft measuring system. The remaining parameters in Table 1, except for $\Delta\alpha$ and $\Delta\beta$ which are derived quantities, are obtained using the gust probe system.

The processing of the raw parameters is shown schematically in Fig. 2. In practice, the processing is repeated a number of times before the final data package, consisting of a WRT (wind, rho-v, temperature) tape, a print-out of means, variances and fluxes, and plotted time series, is produced. The initial processing is done on individual sensor time series which are as long as the actual flight interval. The time series are examined for the presence of missing data, noise spikes and periods of non-stationarity. These intervals are removed and the remaining time intervals are then considered to be separate runs in subsequent processing. In general, no time intervals shorter than about 3 min, corresponding to a path length of about 20 km on a NOAA P-3, are retained for flux calculations.

3. INSTRUMENTAL ACCURACY OF THE NOAA/ERL GUST PROBE SYSTEM

In this section we calculate the instrumental errors associated with the fluctuating meteorological variables and the fluxes when they are obtained from the output of the NOAA/ERL gust probe system. The only other complete calculation of this type was done by Grossman and Bean (1973) over a decade ago. Since then the instrumental errors of some of the raw parameter sensors have been reduced and some of the equations used to calculate the fluctuating

Table 1. Raw parameters used to calculate the fluctuating meteorological variables from the gust probe system. The symbol Δ indicates that the parameter has been linearily detrended and the mean removed. Typical values are given only when needed in calculating the instrumental errors of the fluctuating meteorological variables. The instrumental errors given in the last column incorporate the effects of both sensitivity calibration and instrumental resolution in the measurement of the raw parameters.

Parameter	Definition	Units	Typical value	Instrumental error
$\Delta\theta$	Pitch	rad	0.02	0.0003
$\Delta\phi$	Roll	rad	0.04	0.0003
$\Delta\psi$	Yaw	rad	0.07	0.002
P	Static pressure	mb	1000	0.2
DP	Static pressure-dynamic pressure	mb	60	0.1
T	Temperature	K	300	0.005
N	Scaled refractive index [$N = (n-1) \times 10^6$]	N units	300	0.05
ΔF_α	Force on horizonal vane	g	---	1
ΔF_β	Force on vertical vane	g	---	1
Δa_z	Vertical accel. (c.g.)	$m\ s^{-2}$	---	0.001
Δa_F	Longitudinal accel. (c.g.)	$m\ s^{-2}$	---	0.02
Δa_N	Vertical accel. (boom)	$m\ s^{-2}$	1	0.02
Δa_L	Lateral accel. (boom)	$m\ s^{-2}$	---	0.02
$\Delta\alpha$ *	Vertical angle of attack	rad	0.02	----
$\Delta\beta$ *	Lateral angle of attack	rad	0.05	----

* Derived quantities. See eqs. (9) and (10).

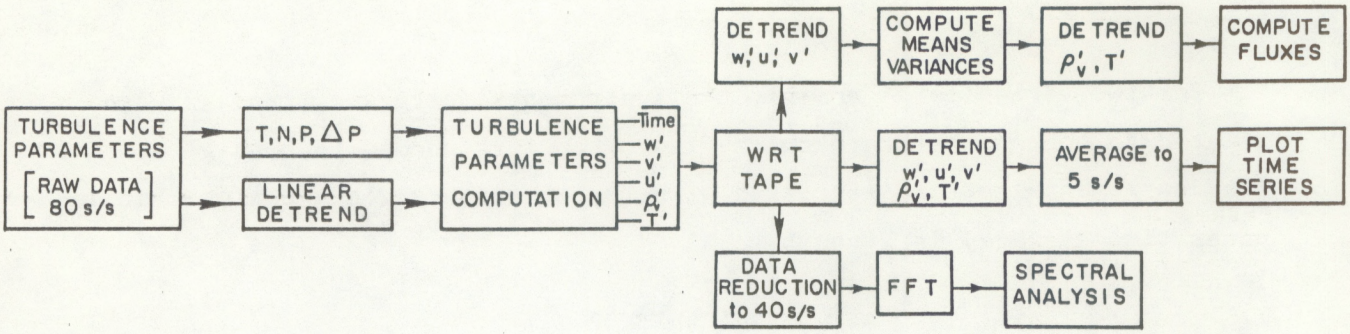

Figure 2.--Flow chart for the reduction of aircraft turbulence data.

meteorological variables have been modified. A new calculation of the instrumental errors is therefore necessary. The results given here supersede those of Grossman and Bean (1973) as well as the instrumental errors quoted by Bean et al. (1976), Gilmer et al. (1978), and Bean and Emmanuel (1980) which are based directly on the results of Grossman and Bean.

Consider two fluctuating meteorological parameters $g'(x_1, x_2, \ldots, x_m)$ and $h'(x_1, x_2, \ldots, x_n)$ which are derived from raw parameters $x_1, x_2, \ldots$. (The parameters g' and h' are obtained from time series that have been linearly detrended with the means removed.) In general, only some of the raw parameters are common to both g' and h'. If ε_i is the instrumental error in the measurement of x_i, then the instrumental error associated with g' is

$$\varepsilon_{g'} = \left[\sum_{i=1}^{m} \left(\frac{\partial g'}{\partial x_i} \varepsilon_i \right)^2 \right]^{1/2} \tag{3}$$

where it has been assumed that the raw parameters are independent variables and that the variations due to instrumental errors are normally distributed (Grossman and Bean, 1973). If g' contains a term $\int_0^\tau x_i dt$, then $\partial g'/\partial x_i$ in (3) is replaced by $(\tau\ \Delta t)^{1/2}$, where τ is the duration of the run and Δt is the time between samples (see the discussion in the Appendix). If g' contains a term $\int_0^\tau x_i x_j dt$, then $(\partial g'/\partial x_i)\varepsilon_i$ in (3) is replaced by

$$(\tau\ \Delta t)^{1/2} \left(x_i^2\ \varepsilon_j^2 + x_j^2\ \varepsilon_i^2 \right)^{1/2}$$

as discussed in the Appendix. For the calculations in this report we use a typical run duration of 5 min (τ = 300 s) and sampling rate of 40 samples s^{-1}

(Δt = 0.025 s.)

For two variables g' and h', the instrumental errors $\varepsilon_{g'}$ and $\varepsilon_{h'}$ are related to one another through the raw parameters common to both g' and h'. The instrumental error associated with the covariance $\overline{g'h'}$ (the overbar denotes time average) is given by

$$\varepsilon_{\overline{g'h'}} = \left[\sum_i \left(\frac{\partial g'}{\partial x_i} \frac{\partial h'}{\partial x_i} \varepsilon_i^2\right)^2\right]^{1/2} \tag{4}$$

where the sum is over the raw parameters common to g' and h' (Grossman and Bean, 1973). In (4), replacements should be made analogous to those discussed above when g' and/or h' contain integrals of the raw parameters.

The fluctuating meteorological variables are T', ρ_v', w', v_a' and u_a' (temperature, water vapor density and vertical, lateral and longitudinal wind components). The subscript a on the horizontal wind components denotes aircraft coordinates. In this system v_a' is positive if directed to the left when facing forward in the aircraft and u_a' is positive if directed to the rear of the aircraft.

T' is measured directly using the small-bead thermistor. The equations relating ρ_v to raw parameters are given in Sec. 2 [eqs. (1) and (2)] and are repeated here for completeness

$$\rho_v = C_1 NT - C_2 P \qquad (g\ m^{-3}) \tag{1}$$

$$N = (n-1) \times 10^6 \tag{2}$$

$$C_1 = 5.81 \times 10^{-4} \quad , \quad C_2 = 4.51 \times 10^{-2} \ .$$

In Table 1, the raw parameters N, T and P are defined and given units that correspond to the constants C_1 and C_2 in (1).

The fluctuations of the wind components are derived from the following small-angle approximations (Axford, 1968)

$$w' = V_T(\Delta\alpha + \Delta\beta\ \Delta\phi - \Delta\theta) + \int_o^\tau \Delta a_z\, dt \qquad (m\ s^{-1}) \quad (5)$$

$$v_a' = V_T(\Delta\beta - \Delta\alpha\ \Delta\phi + \Delta\psi) - \int_o^\tau (\Delta a_L + \Delta a_N\ \Delta\phi + g\Delta\phi)dt \qquad (m\ s^{-1}) \quad (6)$$

$$u_a' = \Delta V_T - \int_o^\tau (\Delta a_F - \Delta a_N\ \Delta\theta - g\Delta\theta)dt \qquad (m\ s^{-1}) \quad (7)$$

where $g = 9.8\ m\ s^{-2}$ is the gravitational acceleration and the raw parameters are defined with appropriate units in Table 1. Since aircraft pitch, roll and yaw are carefully controlled during gust probe measurements, the small angle approximations introduce negligible errors into the calculation of the wind component fluctuations. The symbol Δ indicates that the parameter has been linearly detrended and the mean removed. V_T is the true air speed calculated from

$$V_T = 20.05\ (\gamma T)^{1/2} \qquad (m\ s^{-1})$$

$$\gamma = \left[1.429 + \left(0.275\ \frac{DP}{P} - 0.51\right)\frac{DP}{P}\right]\frac{DP}{P}\ .$$

Since $DP/P \cong 0.06$ (Table 1), we have set

$$\gamma \cong 1.429\ \frac{DP}{P}\ ;$$

therefore

$$V_T \cong C_3\ \left(\frac{DP}{P}\ T\right)^{1/2} \qquad (m\ s^{-1})\ , \quad (8)$$

where $C_3 = 24$. The angle-of-attack parameters are given by

$$\Delta\alpha = \frac{9.274 \times 10^{-3}}{P\gamma}\ (\Delta F_\alpha + 2.04\ \Delta a_N)$$

$$\cong \frac{1}{DP}\ (C_4\ \Delta F_\alpha + C_5\ \Delta a_N) \qquad (rad) \quad (9)$$

$$\Delta\beta = \frac{9.274 \times 10^{-3}}{P\gamma} (\Delta F_\beta + 2.04\ \Delta a_L)$$

$$\cong \frac{1}{DP} (C_4\ \Delta F_\beta + C_5\ \Delta a_L) \qquad \text{(rad)} \qquad (10)$$

where $C_4 = 6.49 \times 10^{-3}$, $C_5 = 1.32 \times 10^{-2}$, and the raw parameters are given in Table 1 with appropriate units. Equations (9) and (10) incorporate the vane constant obtained from wind tunnel calibrations as discussed in Sec. 2.

The derivatives needed in (3) and (4) are obtained by differentiating (1), (2) and (5)-(10) and are evaluated by inserting the typical values of the raw parameters given in Table 1. These are then used in (3) and (4), along with the instrumental errors of the raw parameters in Table 1, to derive the instrumental errors, given in Table 2, associated with the fluctuating meteorological variables and the fluxes. The instrumental errors for the fluctuating horizontal wind components, u' and v', are shown as a single entry in Table 2 since normally the aircraft coordinates are rotated into an along-wind, cross-wind coordinate system that contains linear combinations of u_a' and v_a'. Also shown in Table 2 are the raw parameters that make the largest contributions, often by orders of magnitude, to the instrumental errors of the meteorological variables and fluxes. The instrumental errors for T', ρ_v' and w' are 5% or less of typical values of these variables in the trade wind regime over tropical oceans. For u' and v', the relative error is larger, on the order of 30% of typical values. In the aircraft coordinate system, the instrumental error in u_a' is approximately 0.1 m s^{-1}, contributed to mainly by DP and a_F; for v_a' it is approximately 0.2 m s^{-1}, contributed to mainly by $\Delta\psi$. The instrumental errors in the fluxes are all quite small. The largest relative error, on the order of 2%, occurs for $\overline{w'u'}$ and $\overline{w'v'}$.

4. SPECTRAL CHARACTERISTICS OF THE NOAA/ERL GUST PROBE SYSTEM

Perhaps the best method for validating the fast-response meteorological data derived from the NOAA/ERL gust probe system is spectral analysis. Since 1982, power spectra and cospectra have been produced routinely in order to check the quality of the data during the reduction process (Fig. 2). As we shall see, the spectra of the data used in research are always of high quality, at worst containing white noise that is uncorrelated with vertical velocity fluctuations.

Table 2. Instrumental errors of the fluctuating meteorological variables and the fluxes. Typical values are for the trade wind regime over tropical oceans. A run 5 min (33 km) long is assumed at a sampling rate of 40 samples s^{-1}. The raw parameters that dominate in the calculation of the instrumental errors are given in the last column

Parameter	Units	Typical value	Instrumental error	Main contributing raw parameters
Meteorological variables:				
w'	$m\ s^{-1}$	0.5	0.03	$\Delta\theta$
ρ_v'	$g\ m^{-3}$	0.5	0.01	N, P
T'	K	0.1	0.005	T
u', v'	$m\ s^{-1}$	0.5	0.15	DP, Δa_F, $\Delta\psi$
Fluxes:				
$\overline{w'\rho_v'}$	$W\ m^{-2}$	100	0.0004	P
$\overline{w'T'}$	$W\ m^{-2}$	5	0.000008	T
$\overline{w'u'}$, $\overline{w'v'}$	$N\ m^{-2}$	0.05	0.0009	DP, $\Delta\theta$, Δa_N

A thorough spectral analysis was carried out by Grossman and Bean (1973) (see also Grossman, 1982) on gust probe data obtained aboard the NOAA DC-6 during the Barbados Oceanographic and Meteorological Experiment (BOMEX). The other major boundary layer turbulence experiment aboard the DC-6 occurred during the GARP Atlantic Tropical Experiment (GATE). Reinking (1977) and Greenhut (1981) analyzed the vertical velocity spectra of these data and found that the scales of motion tended to increase with height, as expected, and that these scales were horizontally uniformly distributed in space, indicating the absence of roll vortex structures that were observed in the BOMEX data. Bean and Reinking (1978) presented cospectra corresponding to latent and sensible heat fluxes during GATE.

Some examples of the spectra obtained by Greenhut (1981) from the GATE data are shown in Figs. 3 and 4. They show a decrease with height of the

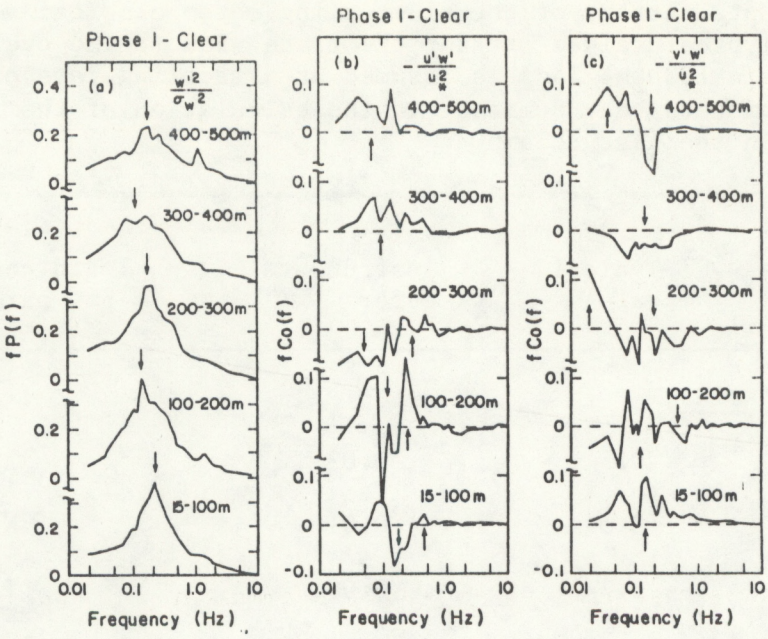

Figure 3.--Composite spectra of turbulence data taken during GATE aboard the NOAA DC-6 over the tropical Atlantic Ocean (from Greenhut, 1981). (a) Power spectra for vertical wind velocity fluctuations. The arrows indicate the peak frequency. (b) Cospectra for the along-wind component of momentum flux. (c) Same as (b) for the cross-wind component.

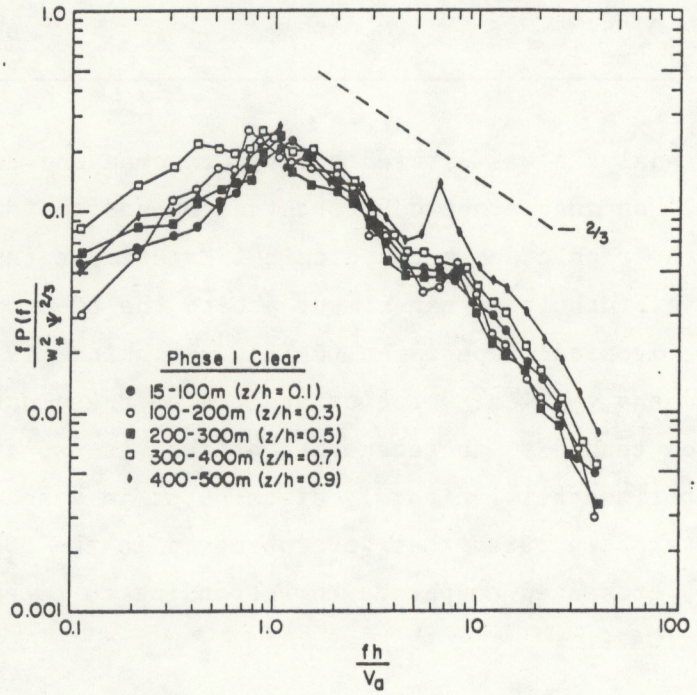

Figure 4.--Normalized spectra of vertical velocity fluctuations as a function of normalized frequency for data taken during GATE (from Greenhut, 1981).

peak frequency in the vertical velocity spectra, corresponding to an increase in the dominant scales of motion (Fig. 3a), and the -5/3 power law in the inertial subrange (Fig. 4). Another feature is the apparent increase with height in the dominant scales of motion which transfer both positive and negative momentum (Fig. 3b,c). The runs used to obtain the spectra and cospectra in Figs. 3 and 4 were carefully selected to avoid the problems discussed by LeMone and Pennell (1980) associated with some of the data obtained by the NOAA/ERL gust probe system aboard the DC-6 during GATE. These problems were completely eliminated when the gust probe system was adapted for use aboard the WP-3D aircraft now being used by NOAA.

The NOAA/ERL gust probe system has been mounted aboard small aircraft for experiments over land, most recently on an Aerocommander as part of the North East Regional Oxidant Study (NEROS) in collaboration with the Environmental Protection Agency. Spectra obtained during this experiment are shown in Fig. 5 for vertical velocity (w), temperature (T) and ozone (O_3) (Greenhut et al., 1984). The -5/3 power dependence of the spectra is evident in the inertial subrange for w and T. The rapid fall-off of the temperature spectra for wavelengths below approximately 50 m is due to the use of a bead thermistor with a cut-off frequency of approximately 3 Hz during this experiment. White noise dominates the ozone signal above about 1 Hz, corresponding to a wavelength of about 70 m. The uncorrelated white noise does not appear in the cospectra for the same data shown in Fig. 6 and therefore does not affect the determination of the ozone flux.

The NOAA WP-3D aircraft have been used as the platforms for experiments over oceans beginning with the North Pacific Experiment (NORPAX) in 1977. Composited cospectra from that experiment are shown in Fig. 7 (Greenhut and Khalsa, 1982). Additional spectra of fast-response data taken aboard the P-3 are shown in Figs. 8-12. Figure 8 shows uncomposited vertical velocity spectra from flights during the Equatorial Pacific Ocean Climate Studies (EPOCS) experiment in 1979, displaying increasing dominant scales of motion (decreasing peak frequencies) with increasing height (Greenhut, 1980). In Fig. 9 composited spectra of the fluctuations of the three wind components

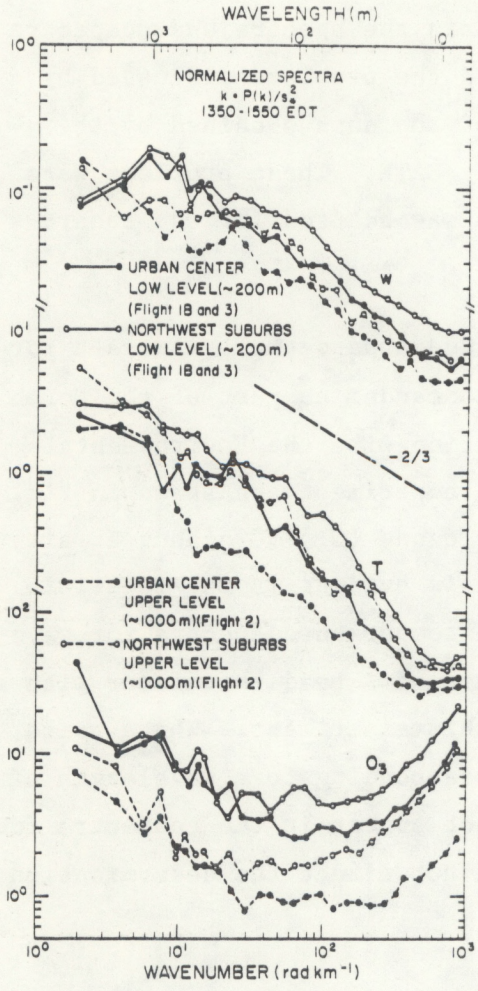

Figure 5.--Power spectra of vertical velocity (w), temperature (T), and ozone (O_3) fluctuations obtained during the NEROS program aboard an Aerocommander in the vicinity of Philadelphia (from Greenhut et al., 1984).

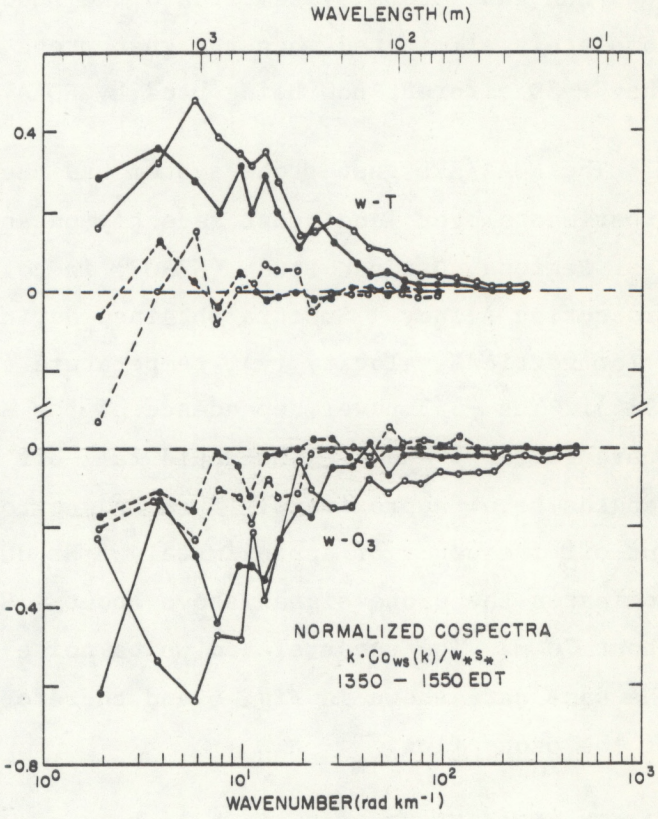

Figure 6.--Cospectra of temperature and ozone with vertical velocity from the NEROS program (from Greenhut, et al., 1984).

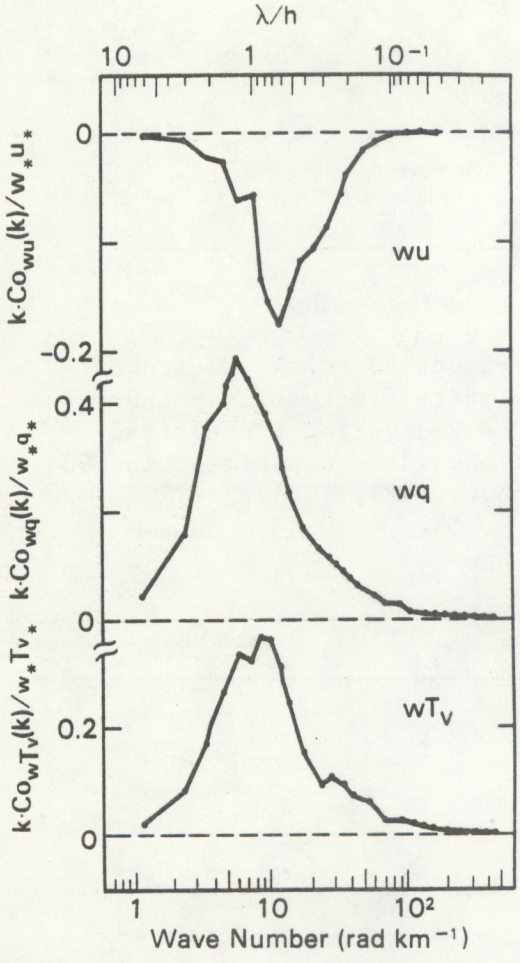

Figure 7.--Composite cospectra corresponding to the fluxes of along-wind momentum, latent heat and buoyancy during the NORPAX experiment (z = 150 m; h ≅ 960 m). Data were taken aboard a NOAA P-3 aircraft over the central tropical Pacific Ocean (from Greenhut and Khalsa, 1982).

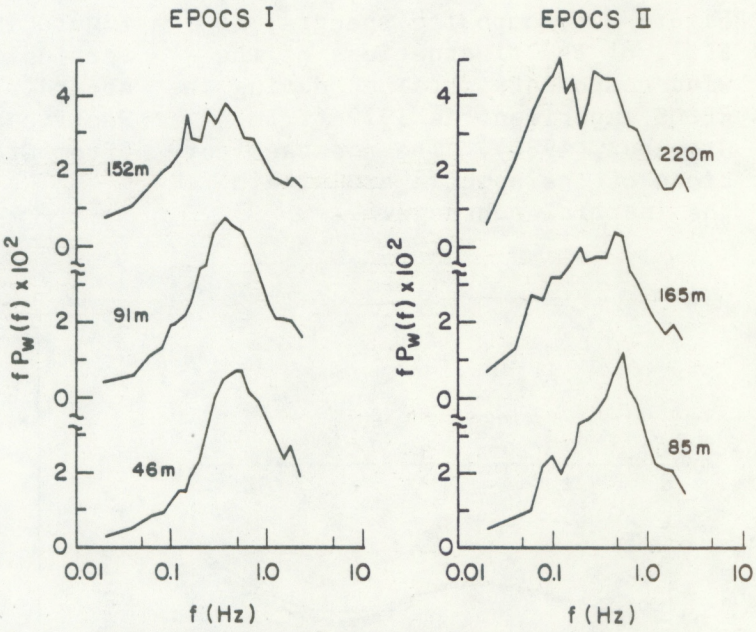

Figure 8.--Individual spectra of vertical velocity fluctuations labeled by height, obtained during the EPOCS experiment in 1979 aboard a NOAA P-3 aircraft over the central equatorial Pacific Ocean (from Greenhut, 1980).

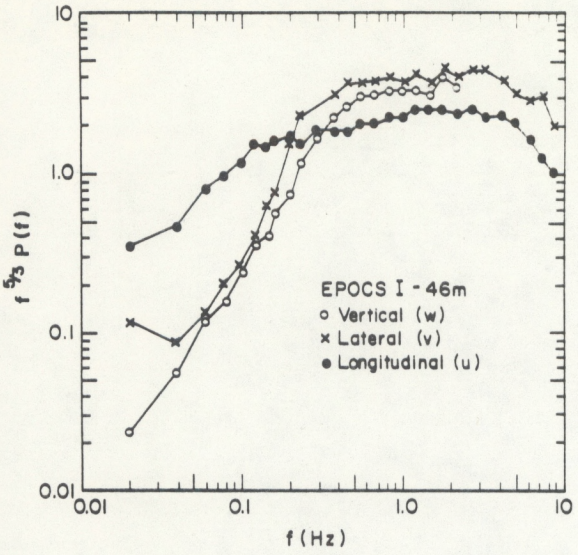

Figure 9.--Composite spectra, $f^{5/3}$ P(f), of the fluctuations of the wind components obtained during the EPOCS experiment in 1979 (from Greenhut, 1980). The constant portions of the spectra are within the inertial subrange.

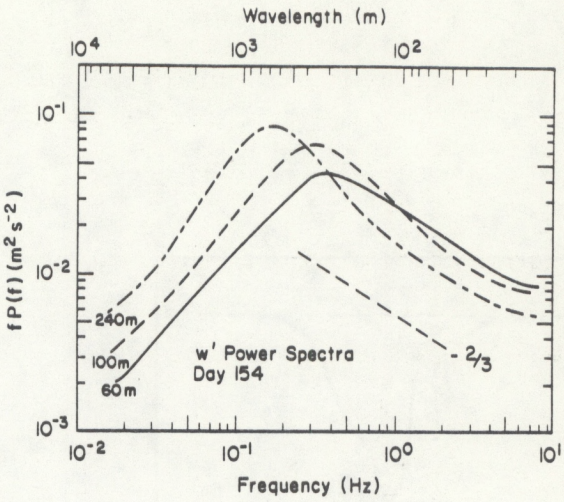

Figure 10.--Smoothed power spectra of vertical velocity fluctuations observed aboard a NOAA P-3 during the central Pacific air chemistry experiment in 1984 (from Greenhut, 1984, 1985).

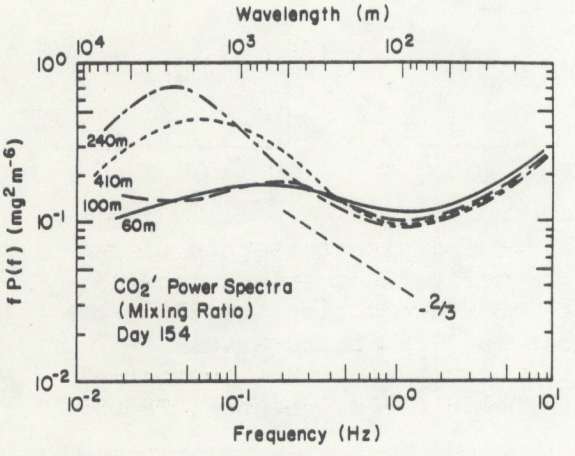

Figure 11.--Same as Fig. 10 for CO_2 fluctuations (from Greenhut, 1984, 1985).

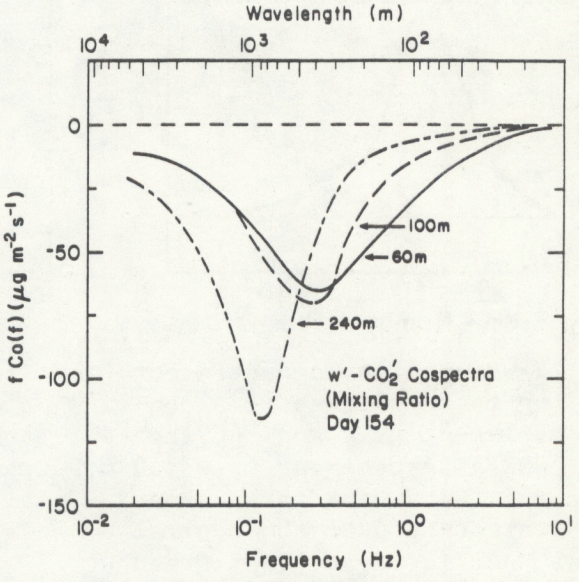

Figure 12.--Smoothed cospectra between CO_2 and vertical velocity fluctuations from the central Pacific air chemistry experiment in 1984 (from Greenhut, 1984, 1985).

observed during the EPOCS experiment are shown as $f^{5/3}$ P(f), emphasizing the inertial subrange which in this plot is the constant value between about 0.3 and 5 Hz. Figures 10-12 are from data obtained during the air chemistry experiment over the central Pacific Ocean during the summer of 1984 (Greenhut, 1984, 1985). The spectra of CO_2 fluctuations at heights of 240 and 410 m in Fig. 11 show a -5/3 power law behavior over the frequency range 0.1 to 0.5 Hz. There is white noise at higher frequencies similar to that observed in the ozone spectra (Fig. 5). As in the case of ozone, the uncorrelated white noise does not affect the measurement of CO_2 flux (Fig. 12).

5. COMPARISON OF EDDY FLUXES OBTAINED FROM THE NOAA/ERL GUST PROBE WITH FLUXES CALCULATED BY THE BULK AERODYNAMIC METHOD

Another test of the validity of the fluxes derived from the NOAA/ERL gust probe system is to compare them with fluxes calculated using the bulk aerodynamic method. This was done by Reinking and Barnes (1981) using data taken during GATE, i.e., when the gust probe system was mounted on the NOAA DC-6. The results of the comparison of latent heat flux measurements during undisturbed weather are shown in Fig. 13 where, from top to bottom, data corresponding to higher aircraft altitudes are progressively excluded. The "ship measurements" are bulk aerodynamic calculations based on the following equation for latent heat flux:

$$E = L_v \bar{\rho} C_E \bar{V}_{10} (\bar{q}_s - \bar{q}_{10}) \qquad (11)$$

where L_v is the latent heat of vaporization, ρ the air density, V_{10} the wind speed at 10 m above the surface, and q_s and q_{10} the specific humidities just above the sea surface and at a height of 10 m, respectively. The overbars indicate time averages. The average length of a run was 96 min and the average wind speed 3.7 m s^{-1} so that an average sample contained about 21 km of path length. The aircraft sampled a comparable length, 23 km, during an average 4 min run at an air speed of 95 m s^{-1}. The bulk transfer coefficient for water vapor, C_E, was chosen to be 1.4×10^{-3} as recommended at the U.S. GATE Workshop (1977).

In Fig. 13, the correlation between the eddy flux measurements from the gust probe and the fluxes calculated by the bulk aerodynamic method increases

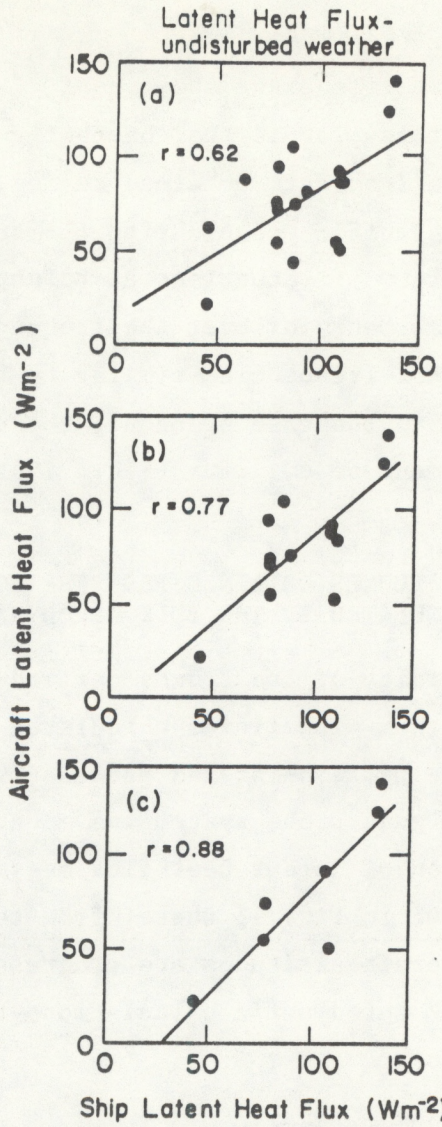

Figure 13.--Comparison of aircraft (DC-6) eddy flux measurements with ship bulk aerodynamic measurements of latent heat flux during GATE (adapted from Reinking and Barnes, 1981). Data from higher aircraft altitudes are progressively excluded. (a) z = 15-153 m, (B) z = 15 and 30 m, (c) z = 15 m. The lines are least-squares fit to the data and the correlation coefficient, r, is given in each case.

as data from higher altitude flights are progressively excluded. Although the lower level flight measurements may be better correlated with the ship measurements, the decreasing size of the sample must also be kept in mind. Reinking and Barnes indicate that the comparison in Fig. 13b is a good compromise between sufficiently large sample size and flights at low enough levels. In this case, the slope of the regression line is 0.91 and the ratio of the ship-to-aircraft mean measurements is 1.18. However, a slope of unity and an

intercept at the origin are well within the 95% confidence intervals derived from a standard t-test.

A somewhat different approach was taken by Greenhut and Bean (1981) using aircraft data obtained during the EPOCS experiment in 1979 when the gust probe system was mounted on a NOAA P-3. In this case, no ship was present at the surface so that the bulk aerodynamic calculation had to be made using parameters observed aboard the aircraft. The calculation used an equation analogous to (11) with ρq_{10} replaced by ρ_{va} (water vapor density), V_{10} replaced by V_a, where the subscript a refers to values at aircraft altitude, and ρq_s replaced by ρ_{vs}, the surface water vapor density derived using the surface temperature measurements from the downward-looking infrared radiometer and assuming saturation. The results for the lowest level flights (at 46 m) are shown in Fig. 14. In this approach, the slope of the least-squares line is used to derive a bulk transfer coefficient, $C_E(46) = 0.91 \times 10^{-3}$. Greenhut and Bean then use surface layer similarity theory to extrapolate this value to the standard height of 10 m and obtain $C_E(10) = (1.10 \pm 0.05) \times 10^{-3}$ which is in good agreement with other determinations of this coefficient over tropical oceans.

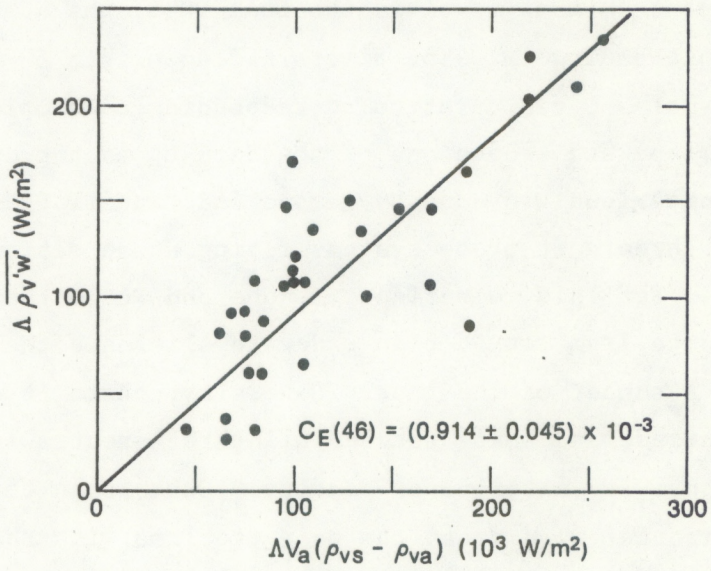

Figure 14.--Comparison of eddy correlation latent heat flux measurements with the bulk aerodynamic formula for data taken at 46 m during the EPOCS experiment in 1979 (from Greenhut and Bean, 1981). Data were taken aboard a NOAA P-3 over the central equatorial Pacific Ocean. The line is a least-squares fit to the data constrained to pass through the origin (r = 0.81).

Because the drag coefficient is strongly dependent on wind speed, Greenhut and Bean (1981) decided that it was best to use the profile of wind speed and along-wind momentum extrapolated to the top of the surface layer (z = 50 m) rather than the values of these parameters measured at the lowest aircraft altitude (46 m) alone. (The uncertainties in the latter contribute to an uncertainty of about ±50% to the drag coefficient.) When the profiles are used, the result for the drag coefficient is $C_D(50) = 1.26 \times 10^{-3}$, which becomes $C_D(10) = 1.55 \times 10^{-3}$ when extrapolated to a height of 10 m using surface layer similarity theory. This value of $C_D(10)$ is in excellent agreement with previous determinations of the drag coefficient at moderate wind speeds over oceans (e.g., Garratt, 1977).

6. COMPARISON OF THE NOAA/ERL GUST PROBE SYSTEM WITH OTHER GUST PROBE SYSTEMS

The NOAA/ERL gust probe system has been flown simultaneously with other gust probe systems for intercomparisons in at least three experiments: GATE in 1974, the Storm Transfer and Response Experiment (STREX) in 1980, and FIRE 85/DYCOMS based in San Diego in 1985. Data from the latter experiment have not yet been analyzed.

The GATE intercomparison involved the NOAA DC-6, the NCAR L-188 and a C-130 from the United Kingdom. The aircraft flew within 50-100 m of each other during legs of 5-6 min duration corresponding to sample lengths of 29-34 km. After separate reductions of the data by each group, the final analysis and intercomparison was done by LeMone and Pennell (1980). Composite spectra from the three gust probe systems flying at an altitude of 305 m are shown in Fig. 15. For this comparison, LeMone and Pennell have filtered the horizontal wind data from the DC-6 in order to eliminate the low frequency noise present in a number of the runs. Generally, there is excellent agreement in magnitude and shape between all three spectra for the wind components, temperature and water vapor density. Other than the low frequency noise in the horizontal wind data, the only problems with the NOAA data in this experiment were a too rapid fall-off at high frequencies for the longitudinal velocity (u) and a high bias at low frequencies for the vertical velocity (w). The latter was due to slightly different procedures for calculating the aircraft vertical velocity. The slower fall-off of the temperature

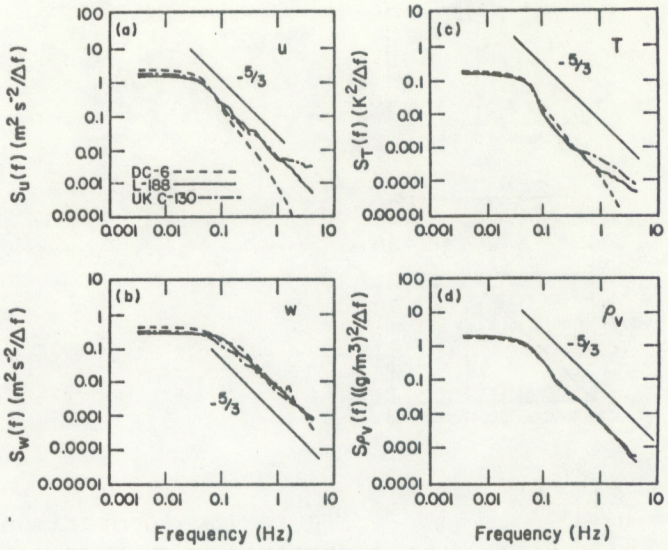

Figure 15.--Composite power spectra of turbulence data taken aboard the NOAA DC-6, NCAR L-188 and the UK C-130 during GATE at an altitude of 305 m (adapted from LeMone and Pennell, 1980): (a) longitudinal velocity, (b) vertical velocity, (c) temperature and (d) water vapor density.

spectra for the NCAR and UK data at high frequencies is due to salt contamination of their temperature sensors.

Figure 16 shows an intercomparison of fluxes measured simultaneously by the three gust probe systems during GATE. The scatter is typical of flux intercomparisons (see Fig. 19) and is mainly due to inhomogeneities in the boundary layer turbulence field over distances as small as the 100-200 m separation between the three aircraft. Scatter in the comparison of the fluxes of temperature and moisture is also contributed to by salt contamination that occurred on the temperature sensors on the L-188 and C-130. The scatter is much reduced when a number of flux runs are averaged together for each of the gust probe systems. This can be seen in Fig. 17 where consistent flux profiles are obtained using the output of two gust probe systems simultaneously.

In 1980 during STREX, a flight was made by a NOAA P-3 and the NCAR Electra over the northern Pacific Ocean at 150 m above sea level to compare flux and other meteorological measurements. Figure 18 shows a comparison of the friction velocity, $u_* = (-\overline{u'w'})^{1/2}$, calculated from the data from these flights. The agreement is fairly good, but it must be remembered that the scatter in the fluxes is reduced here because the square root has been taken.

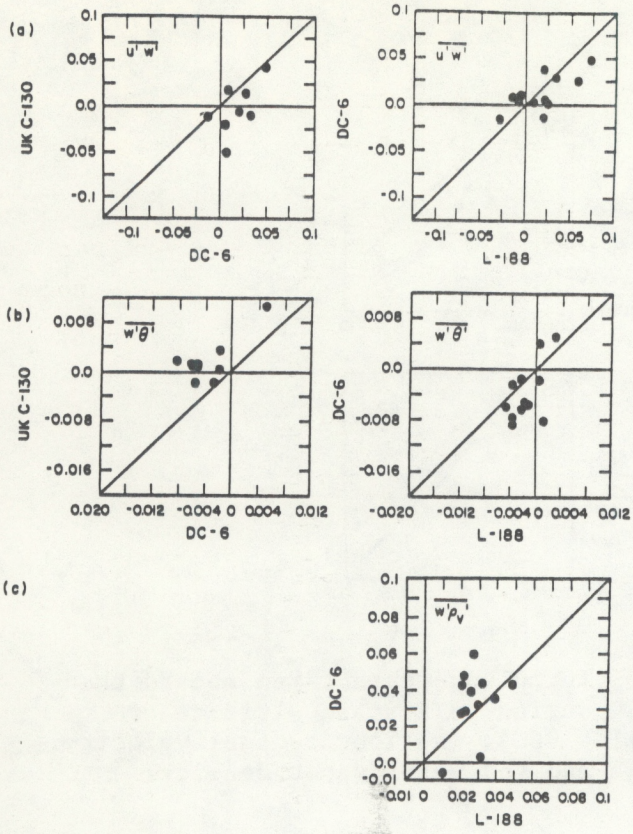

Figure 16.--Comparison of flux measurements between three aircraft during GATE: NOAA DC-6, NCAR L-188 and UK C-130 (adapted from LeMone and Pennell, 1980). Units are mks except $\overline{w'\rho_v'}$ which is g m^{-2} s^{-1}

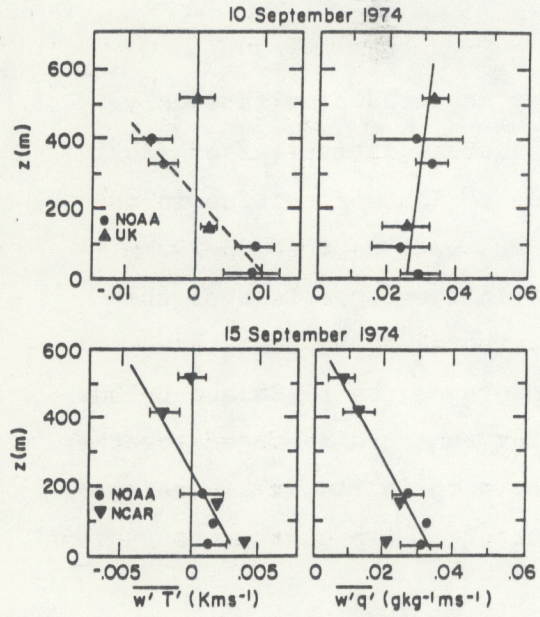

Figure 17.--Profiles of temperature and humidity flux for two days in GATE (adapted from LeMone and Pennell, 1980). The points with standard deviation bars are averages over two or or more runs.

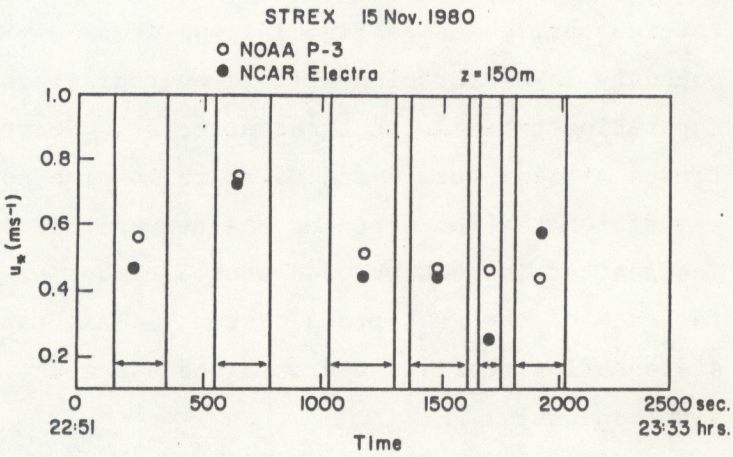

Figure 18.--Comparison of friction velocity $u_* = (-\overline{u'w'})^{1/2}$, obtained aboard a NOAA P-3 and the NCAR Electra during STREX in 1980 (adapted from Oncley et al., 1981). The vertical lines correspond to the starting and ending times for calculating u_*.

Direct comparisons of the fluxes of momentum, temperature, water vapor and virtual temperature are shown in Fig. 19. The scatter is similar to that observed in the GATE data in Fig. 16 and is probably again due to inhomogeneities in the turbulence field over the distance between and aircraft. A typical sample length of about 22 km for a run of 3.3 min (see Fig. 18) is not long enough to average out the different turbulence structures encountered by two separated aircraft.

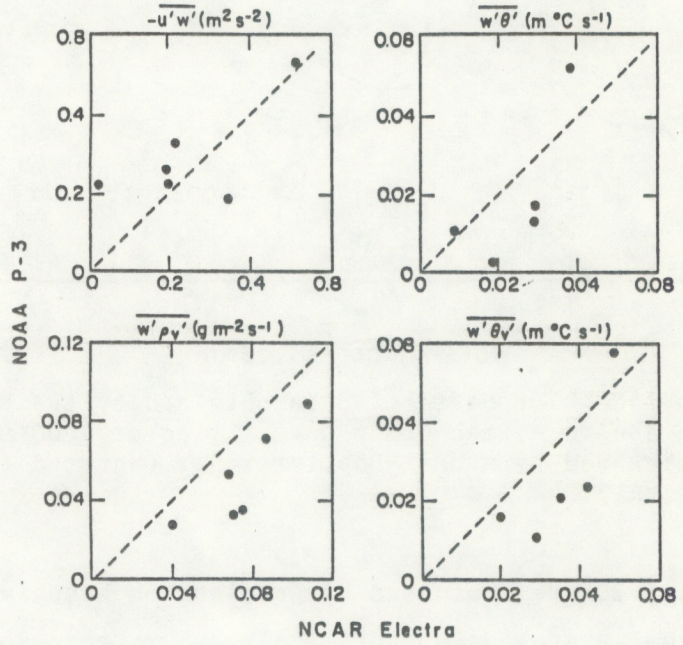

Figure 19.--Comparison of flux measurements made aboard a NOAA P-3 and the NCAR Electra at 150 m above sea level during STREX (adapted from Oncley et al., 1981).

7. COMPARISON OF THE NOAA/ERL GUST PROBE SYSTEM WITH A DUAL-DOPPLER RADAR

The NOAA/ERL gust probe system was mounted aboard a Beechcraft Duke aircraft in 1977 and flown through roll vortices simultaneously with observations made by a dual-Doppler radar (Reinking et al., 1981). Composite spectra from both systems for crosswind (v') fluctuations are shown in Fig. 20 for aircraft data taken at 1000 m AGL. The aircraft flew perpendicular to the wind direction and therefore v' is the wind component along the aircraft axis. The roll vortices were aligned nearly along the wind direction so the aircraft direction was nearly perpendicular to the axis of the vortices.

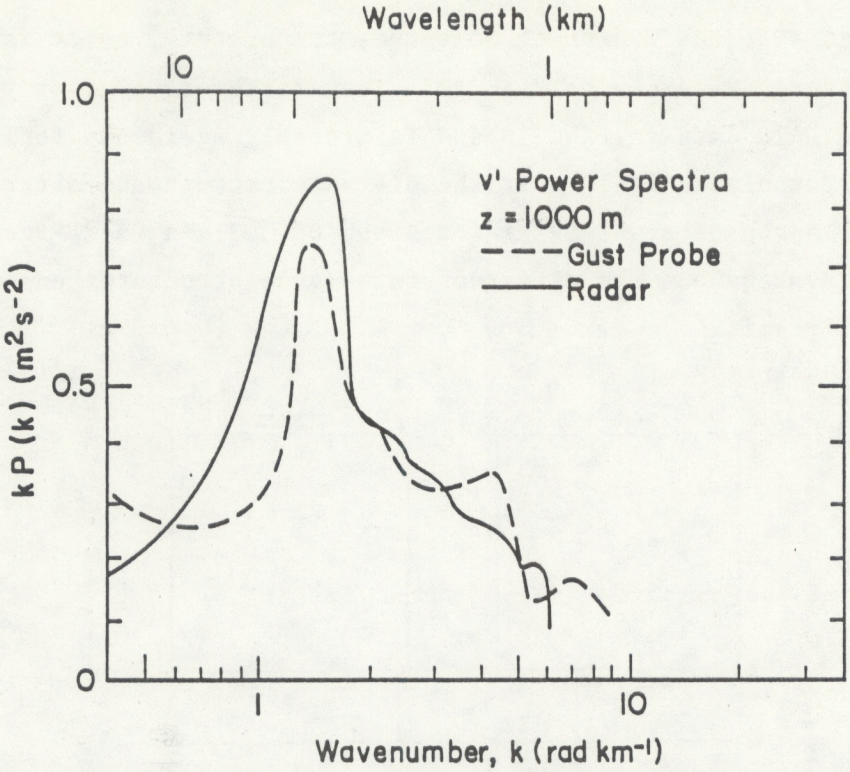

Figure 20.--Comparison of spectra of data obtained by the NOAA/ERL gust probe system aboard a Beechcraft Duke flying at 1000 m AGL with spectra of data obtained by a dual-Doppler radar (adapted from Reinking et al., 1981).

The spectra in Fig. 20 are dominated by wavelengths associated with the spacing of the vortices, averaging approximately 4.5 km corresponding to a frequency of 0.02 Hz at an aircraft speed of 85 m s^{-1}. The spectra compare well at all wavelengths down to 1 km which was the cut-off for the dual-Doppler radar data. This cut-off corresponds to a frequency of 0.09 Hz for the aircraft data.

8. SUMMARY AND CONCLUSIONS

The last complete calculation of the instrumental errors associated with the NOAA/ERL gust probe system was done over a decade ago (Grossman and Bean, 1973), and since then the accuracy of some of the components of the system has been improved. The results of an updated calculation are given in Table 2. The largest instrumental errors in the flux measurements, approximately 2%, occur for momentum flux. As we have seen in Figs. 16, 18 and 19, the natural variability of the flux measurements averaged over path lengths less than about 35 km is much greater than the instrumental errors given in Table 2.

The power spectra and cospectra in Figs. 3-12 show that data from the gust probe system are well behaved; there is little, if any, noise contamination in the frequency band 0.01 to 10 Hz. In all cases, there is a well-defined inertial subrange and the dominant length scales increase with height as expected. A comparison of the eddy fluxes obtained from the gust probe system with fluxes calculated using the bulk aerodynamic method shows that the resulting bulk transfer coefficients are well within the range of acceptable values for fluxes over oceans.

A careful examination of the results of intercomparisons of the NOAA/ERL gust probe system with those of NCAR and the United Kingdom (LeMone and Pennell, 1980; Oncley, 1981) shows that the NOAA/ERL system works as well as the other systems. As mentioned above, the variability of the fluxes, even when averaged over a path length as long as 35 km, makes direct comparisons of flux measurements very difficult. However, when a number of flux runs at a given height are averaged together, as in Fig. 17, the resulting profiles are quite consistent when two different gust probe systems are used simultaneously.

The results of this report indicate that the NOAA/ERL airborne gust probe system is a reliable tool for measuring turbulence parameters and that data obtained from this system can be used with confidence in atmospheric boundary layer research.

ACKNOWLEDGMENT

We thank E. Westwater for suggesting the method given in the Appendix for calculating instrumental errors due to integral terms.

10. REFERENCES

Axford, D. N., 1968: On the accuracy of wind measurements using an inertial platform in an aircraft, and an example of a measurement of the vertical mesostructure of the atmosphere. J. Appl. Meteor., 7, 645-666.

Bean, B. R., and E. J. Dutton, 1966: Radio Meteorology. NBS Monograph 92, available from Superintendent of Documents, U.S. Govt. Printing Office, Washington, DC 20402, 435 pp.

Bean, B. R., and C. B. Emmanuel, 1980: Aircraft. In Air-Sea Interaction: Instruments and Methods, F. Dobson, L. Hasse and R. Davis (Eds.), Plenum, New York, 571-587.

Bean, B. R., and R. F. Reinking, 1978: Marine turbulent boundary layer fluxes of water vapor, sensible heat and momentum during GATE. In Turbulent Fluxes Through the Sea Surface, Wave Dynamics and Prediction. A. Favre and K. Hasselmann (Eds.), Plenum, New York, 21-33.

Bean, B. R., R. O. Gilmer, R. F. Hartmann, R. E. McGavin and R. F. Reinking, 1976: Airborne measurement of vertical boundary layer fluxes of water vapor, sensible heat and momentum during GATE. NOAA Tech. Memo. ERL WMPO-36, NOAA Environmental Research Laboratories, Boulder, CO, 83 pp.

Bingham, G. E., and J. H. Shinn, 1983: Tracking the global carbon cycle. In Energy and Technology Review, August Issue, Lawrence Livermore National Laboratory, Livermore, CA, 1-10.

Garratt, J. R., 1977: Review of drag coefficients over oceans and continents. Mon. Wea. Rev., 105, 915-929.

Gilmer, R. O., and R. E. McGavin, 1977: A small aircraft gust-probe system. NOAA Tech. Memo. ERL WMPO-41, NOAA Environmental Research Laboratories, Boulder, CO, 14 pp.

Gilmer, R. O., R. E. McGavin, and R. F. Reinking, 1978: A small aircraft gust-probe system for studies of boundary layer convection and transport. Preprints: Fourth Symposium on Meteorological Observations and Instrumentation, Denver, CO. American Meteorological Society, Boston, 426-432.

Greenhut, G. K., 1980: Aircraft measurements of boundary layer turbulence over the central equatorial Pacific Ocean. EPOCS-NORPAX Data Display Workshop, University of California, San Diego.

Greenhut, G. K., 1981: Analysis of aircraft measurements of momentum flux in the subcloud layer over the tropical Atlantic Ocean during GATE. Bound.-Layer Meteor., 20, 75-100.

Greenhut, G. K., 1983: Aircraft measurements of the flux of CO_2 over the Caribbean Sea. IUGG XVIII General Assembly, Inter-Disciplinary Symposia,

Program and Abstracts, Vol. 2, Hamburg, 835.

Greenhut, G. K., 1984: Aircraft measurements of CO_2 eddy fluxes over the central equatorial Pacific Ocean. EOS, 65, 961.

Greenhut, G. K., 1985: Turbulent transport of CO_2 in the marine atmospheric boundary layer. IAMAP/IAPSO Joint Assembly, Honolulu, American Geophysical Union, Washington, D.C., 34.

Greenhut, G. K., and B. R. Bean, 1981: Aircraft measurements of boundary layer turbulence over the central equatorial Pacific Ocean. Bound.-Layer Meteor., 20, 221-241.

Greenhut, G. K., and S. J. S. Khalsa, 1982: Updraft and downdraft events in the atmospheric boundary layer over the equatorial Pacific Ocean. J. Atmos. Sci., 39, 1803-1818.

Greenhut, G. K., J. K. S. Ching, R. Pearson, Jr., and T. P. Repoff, 1984: Transport of ozone by turbulence and clouds in an urban boundary layer. J. Geophys. Res., 89, 4757-4766.

Grossman, R. L., 1982: An analysis of vertical velocity spectra obtained in the BOMEX fair-weather, trade wind boundary layer. Bound.-Layer Meteor., 23, 323-357.

Grossman, R. L., and B. R. Bean, 1973: An aircraft investigation of turbulence in the lower layers of a marine boundary layer. NOAA Tech. Report ERL 291-WMPO 4, NOAA Environmental Research Laboratories, Boulder, CO, 137-155.

Khalsa, S. J. S., and G. K. Greenhut, 1985: Conditional sampling of updrafts and downdrafts in the marine atmospheric boundary layer. J. Atmos. Sci., 42, 2550-2562.

LeMone, M. A., and W. T. Pennell, 1980: A comparison of turbulence measurements from aircraft. J. Appl. Meteor., 19, 1420-1437.

McGavin, R. E., and M. J. Vetter, 1965: Radio refractometry and its potential for humidity studies. In Humidity and Moisture, Measurement and Control

in Science and Industry, Vol. 2, Applications. A. Wexler (Ed.), Reinhold, New York, 553-560.

Oncley, S., C. Friehe, B. Bean, and W. L. Jones, 1981: Intercomparisons of aircraft data during STREX. In STREX Workshop Report. M. Miyake and E. E. Recker (Eds.), University of Washington, Seattle, WA, 119-130.

Pearson, R., Jr., and D. H. Stedman, 1980: Instrumentation for fast response ozone measurements from aircraft. Atmos. Tech., 12, 51-55.

Reinking, R. F., 1977: The statistical nature of vertical eddy motion during GATE. Conference Papers: Eleventh Technical Conference on Hurricanes and Tropical Meteorology, Miami Beach. American Meteorological Society, Boston, 232-237.

Reinking, R. F., and G. Barnes, 1981: A comparison of tropical oceanic heat fluxes determined by airborne eddy correlation and shipboard bulk aerodynamic techniques. Bound.-Layer Meteor., 20, 353-370.

Reinking, R. F., R. J. Doviak, and R. O. Gilmer, 1981: Clear-air roll vortices and turbulent motions as detected with an airborne gust probe and dual-Doppler radar. J. Appl. Meteor., 20, 678-685.

U.S. GATE Central Program Workshop, 1977: Report of the Workshop, Boulder, CO. Available from the National Center for Atmospheric Research, Boulder, CO, 723 pp.

APPENDIX

CONTRIBUTION TO INSTRUMENTAL ERRORS FROM INTEGRALS OF RAW PARAMETERS

Equations (5), (6) and (7) for the fluctuations of the wind components contain integrals of either one raw parameter or the product of two raw parameters. Since the actual observations are discrete, the integrals can be written as sums

$$\int_0^\tau x_i dt = x_i(t_1)\Delta t + x_i(t_2)\Delta t + \ldots + x_i(t_n)\Delta t$$

$$= \Delta t[x_i(t_1) + x_i(t_2) + \ldots + x_i(t_n)] \qquad \text{(A1)}$$

$$\int_0^\tau x_i\, x_j\, dt =$$

$$\Delta t[x_i(t_1)x_j(t_1) + x_i(t_2)x_j(t_2) + \ldots + x_i(t_n)x_j(t_n)] \qquad \text{(A2)}$$

where τ is the total duration of the run and Δt is the time interval between each observation. Let ε_i be the instrumental error in the measurement of x_i and $\varepsilon(\text{int } x_i)$ and $\varepsilon(\text{int } x_i\, x_j)$ be the instrumental errors associated with the integrals (A1) and (A2). If the variations due to the instrumental errors are assumed to be normally distributed, then

$$[\varepsilon(\text{int } x_i)]^2 = (\Delta t)^2\, [\varepsilon_i^{\,2}(t_1) + \varepsilon_i^{\,2}(t_2) + \ldots + \varepsilon_i^{\,2}(t_n)]$$

$$= \nu(\Delta t)^2\, \varepsilon_i^{\,2} \qquad \text{(A3)}$$

$$[\varepsilon(\text{int } x_i\, x_j)]^2 = (\Delta t)^2[\varepsilon_{ij}^2(t_1) + \varepsilon_{ij}^2(t_2) + \ldots + \varepsilon_{ij}^2(t_n)]$$

$$= \nu(\Delta t)^2\, \varepsilon_{ij}^2 \qquad \text{(A4)}$$

where ν is the total number of observations in the run and it is assumed that the ε_i and ε_{ij} are independent of time. In (A4), $\varepsilon_{ij}^{\,2}$ is analogous to the variance of the product $x_i\, x_j$ and therefore

$$\varepsilon_{ij}^2 = x_i^{\,2}\, \varepsilon_j^{\,2} + x_j^{\,2}\, \varepsilon_i^{\,2}\,. \qquad \text{(A5)}$$

Since $\nu = \tau/\Delta t$, (A3) and (A4) become

$$\varepsilon(\text{int } x_i) = (\tau\Delta t)^{1/2}\ \varepsilon_i \tag{A6}$$

$$\varepsilon(\text{int } x_i\ x_j) = (\tau\Delta t)^{1/2}(x_i^{\,2}\ \varepsilon_j^{\,2} + x_j^{\,2}\ \varepsilon_i^{\,2})^{1/2}\ . \tag{A7}$$